Injection of a relativistic electron beam into a high intensity optical lattice

M Hadj-Bachir, Igor Andriyash, B. Barbrel, Vladimir Tikhonchuk, Emmanuel d'Humières, Philippe Balcou

Injection of a relativistic electron beam into a high intensity optical lattice

M. Hadj-Bachir,[1,*] I.A. Andriyash,[2] B. Barbrel,[1] V.T. Tikhonchuk,[1] E. d'Humières,[1] and Ph. Balcou[1]

[1] *Univ. Bordeaux, CNRS, CEA, CELIA, UMR 5107, F33400 Talence,France*

[2] *Synchrotron SOLEIL, L'Orme des Merisiers, Saint-Aubin, BP 48, 91192 Gif-sur-Yvette CEDEX, France*

We present a numerical study of the injection and trapping process of a bunch of relativistic free electrons into a transverse high intensity optical lattice. We unravel different injection regimes depending on the characteristic length scale of the onset of the optical lattice, and explore how the characteristics of the electron beam and of the high intensity lattice affect the trapping rate. The average transverse kinetic energy, and the induced longitudinal energy broadening are studied. The analysis of the transverse phase space exhibits a complex behavior, leading to inhomogeneities that may affect the amplification dynamics of X-ray Free Electron Laser.

I. INTRODUCTION

The possibility to use intense laser to wiggle relativistic electrons and to trigger a free electron laser process has stimulated a number of studies [1, 2]. The undulator period is given by the laser wavelength, in the micrometer range, which should allow one to obtain X-ray beams on the basis of weakly relativistic electrons, with typical energies of few tens of MeV only, making this scheme extremely appealing in terms of compacity and flexibility. Advanced optical schemes are currently considered, in order to trigger the amplification of backscattered radiation, either in a Thomson [3] or Compton [4] regime. However, the practical conditions on the electron bunch parameters, in terms of monoenergeticity, emittance, divergence, and on those of the laser beams: intensity constancy, are so stringent that no practical realization of such amplification has been achieved yet [3].

To overcome these limitations we have proposed a new concept of compact XFEL based on a combination between the physics of free electron lasers, laser-plasma interaction, and nonlinear optics [5]. This conceptual scheme, called "Raman XFEL", is based on the interaction between relativistic free electrons and a transverse optical lattice at laser intensities high enough to induce the so-called strong field Kapitza-Dirac effect [6, 7]. As depicted in Figure 1, the high intensity optical lattice is obtained by crossing two laser beams, inducing an interference pattern, on which the relativistic electrons are incident. The physics of the interaction between an electron bunch and such an optical lattice is of interest by itself, with rich dynamical behaviours and polarization-dependent phenomena [8, 9]. In particular, the electrons may be transversely trapped within the ponderomotive potential, oscillate at low frequency, and thus induce a scattering process similar to the stimuated Raman scattering in plasmas [5, 10]. In terms of a parametric process, the wiggler – the light lattice – represents the pump wave, the idler is the induced collective transverse electron oscillation or beam-plasma wave mode, and the output signal is the daughter wave.

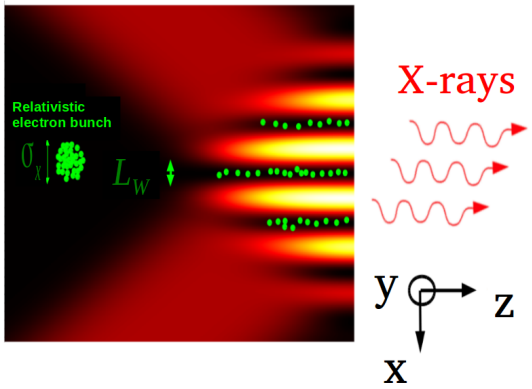

FIG. 1. Proposed configuration for a Raman X-ray Free Electron Laser: the two laser beams interfere creating a series of potential wells, and the color code from black to yellow indicates the height of the ponderomotive potential due to the laser standing wave. The relativistic electron bunch is represented here with a group of green dots.

Analytical and numerical studies based on a kinetic theory have demonstrated that this system can exhibit a significant gain [11, 12], provided that one can inject a sufficient number of electrons into the optical lattice and maintain the stable interaction over a sufficient length. Moreover, another lies in the fact that the electrons are guided within the interaction region, that can be made to extend over several typical divergence lengths.

The longitudinal and transverse temperatures and the electron charge density are expected to play an important role in the beam dynamics, and hence in the X-rays amplification. For this, the present article aims at studying numerically in more details how the injection of free relativistic electrons into an optical lattice depends on the collective parameters of the relativistic electron bunch (divergence, electron kinetic energy, energy spread, emittance), as well as on those of

* hadjbachir@celia.u-bordeaux1.fr

the optical lattice (intensity, interaction length, width of the potential well).

This study is based on a dedicated numerical tool, dubbed RELIC. We first present the specificities of the physical situation. Then we summarize the approximations used and present the set of equations used for the code. We focus on the electron trapping rate, mean transverse energy and the induced longitudinal slowing down. We explore the rich dynamics seen in phase space, and its relations to the amplification process of a Raman XFEL. A general discussion and our concluding remarks are presented in the last section.

II. DESCRIPTION OF THE PHYSICAL CASE

The conceptual scheme of the Raman XFEL is illustrated in Figure 1. It implies to overlap in vacuum two identical laser pulses with the same frequency, identical linear polarisation vectors perpendicular to the incidence plane, and crossing with an angle 2θ. The beam interaction produces a spatially periodic light potential resembling a series of parallel half-pipes, in which free relativistic electron bunches issued from Laser Plasma Accelerator (LPA) [14, 15] or traditional Linear Accelerators (LINAC) [16, 17] can be trapped.

In this study of the electron dynamics, we consider a relatively simple, generic laser intensity profiles and concentrate on the essential features of the physics of injection, independently of sophistications depending on experimental implementations. The advanced optical setups such as the so-called inhomogeneous waves [5], and of spatial inhomogeneties due to real beam profiles, will be addressed in future studies. We therefore consider here an ideal optical lattice with a laser field distribution consisting of an initial field-free zone by which the relativistic electrons are incident, followed by a ramp of linearly increasing intensity, whose length L_R corresponds to the growth of the lattice potential from zero to its maximum value (Fig 2(a)). The region at the end of the linear ramp is assumed to be a plateau of constant intensity (Fig 2(b)). For the sake of simplicity, we will not consider the effect of the ponderomotive force in the second transverse direction y, assuming an infinite lattice along this transverse axis.

As a model case, let us consider a relativistic electron bunch with an average Lorentz factor γ advancing along the z-axis through an optical lattice. The electrons interacting with a spatially non-uniform laser field are subject to a ponderomotive force $F_p = -\bigtriangledown V_{pot}$, which, for each interaction region can be expressed as:

$$V_{pot}(x,z) = 0 \quad \text{for } z < 0,$$

$$V_{pot}(x,z) = \frac{m_e c^2 {a_0}^2}{2\gamma}\left(1-\cos(2k_\perp x)\right)\frac{z}{L_R} \quad \text{for } 0 < z < L_R,$$

$$V_{pot}(x,z) = \frac{m_e c^2 {a_0}^2}{2\gamma}\left(1-\cos(2k_\perp x)\right) \quad \text{for } z > L_R$$

where a_0 is the normalized vector potential, m_e- the electron mass, γ- the electron Lorentz factor, c- the speed of light and $k_\perp = \frac{2\pi}{\lambda_0}\sin\theta$- the transverse wave vector.

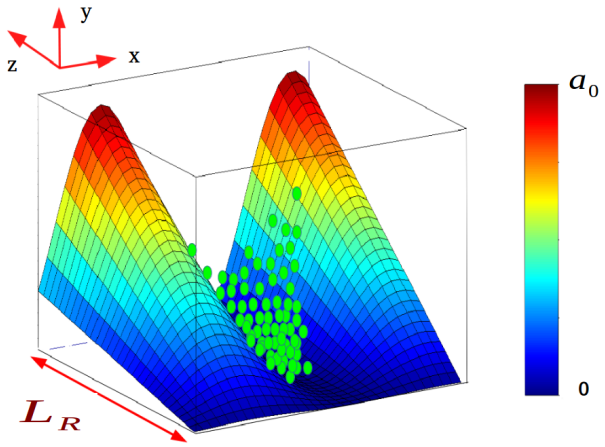

(a)Schematic representation of the linear ramp. The potential grows from zero (blue) to its maximum value a_0 (red) on a scalelength L_R.

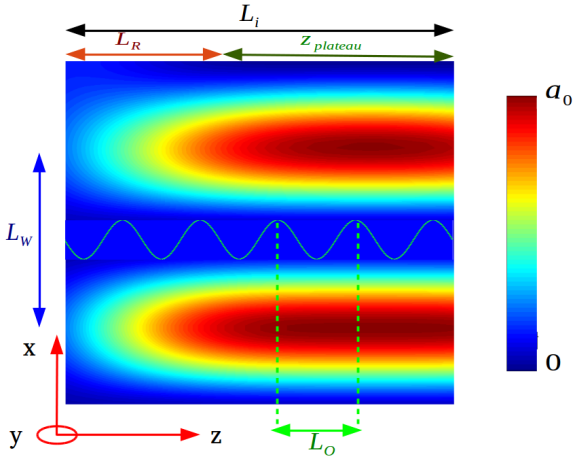

(b)Schematic representation of a trapped electron trajectory in a ponderomotive potential well. L_O is the spatial electron oscillation period; L_W is the width of the optical well; the total interaction length $L_i = L_R + z_{plateau}$ is the sum of the linear ramp length L_R and of the plateau length area $z_{plateau}$

FIG. 2. Schematic representation of the two interaction regions: linear ramp and plateau area.

In the transverse plane, the interaction geometry depends in the most general case on the relative sizes and

positions of the bunch and the optical lattice. The transverse size of the relativistic electron bunch is defined as: $\sigma_x = \epsilon_N/(\gamma\Sigma)$, where ϵ_N and Σ are the normalized emittance and the RMS divergence at the accelerator end, respectively. We introduce a divergence length along which the electron bunch remains collimated, as:

$$L_{div} = \gamma {\sigma_x}^2/\epsilon_N. \quad (1)$$

This length must be considered for electron bunches of large divergences, in which case it may fall short with respect to the ramp length L_R.

Owing to both the initial size σ_x and to the electron divergence, a part of electrons may therefore not see the optical lattice which is limited by the spot size of the laser. We do not attempt to describe this obvious geometric factor, and we will consider that the optical lattice is infinite in both transverse directions x and y. The height of the effective energy of the potential wells after the injection area ($z > L_R$) is considered uniform and equal to a_0^2/γ.

The electron bunch can be injected into a single well or in multiple wells depending on the ratio σ_x/L_W, where $L_W = \lambda_0/2\sin\theta$ is the width of the potential well. Recent developments in laser plasma acceleration have shown a reduction in divergence of electron bunches using a plasma lens [18, 19]. This could help to have a low divergence electron bunch and achieve a single well injection.

The spatial oscillation period of an electron in the ponderomotive potential well is given by $L_O = c\cdot\Omega_0^{-1}$ where Ω_0 is the electron oscillation frequency given by Eq. 7. If the length of the injection region is much longer than L_O, injection proceeds in a smooth, adiabatic fashion; conversely, if the injection region is much shorter than L_O, then the beam is interacting in a very sudden way. We thus define an adiabatic parameter as:

$$\Gamma_{ad} = \frac{L_R}{L_O}. \quad (2)$$

This parameter allows us to separate two injection regimes, namely fast injection, and adiabatic injection [10]. It will also appear as instrumental to study how the transverse energy and the amplification depend on the injection regime.

The injection regime is directly related to the ramp length which modifies significantly the electron dynamics in the tranverse phase space. The distribution of electrons in the phase space is particularly connected to the trapping of an electron in the potential well and to the electron oscillation frequency. This allows us to define the optimum parameters for a better trapping rate of electrons in the ponderomotive potential wells and to link them to the Raman X-ray amplification.

III. NUMERICAL MODEL

A. RELIC code

We have developed a particle simulation code, dubbed RELIC, to study the dynamics of a relativistic electron bunch issued either from LINAC, or obtained by LPA in the laboratory frame. The code describes the dynamics of all electrons of a macroscopic bunch, including the broadening induced by the entrance into an interaction region. It is simple enough requiring a relatively small computing time, and is capable to cope with future refinements, such as the spatial inhomegeneities of real laser beams. It describes the electron motion in the ponderomotive potential accounting for the relativistic mass increase in the three-dimensional phase space. The code provides access to macroscopic beam parameters such as the emittance or the Twiss parameters (see section IV B).

RELIC is a particle tracker code similar to the ones used in the accelerator codes to model the particle beam transport such as PARMELA [20] or ASTRA [21]. RELIC can simulate the particles transport in different laser geometries, and successive steps (free propagation, standing-wave, travelling wave-structures) in either two and three space dimensions. As an output, the code gives the physical parameters of the electron beam, which can then be used in the Particle-In-Cell (PIC) modeling of the scattered light amplification. In our study we will use the code EWOK designed to simulate the coupling between electron oscillations, laser and scattered electromagnetic fields in the electron rest frame [11].

In this paper we use the 2D version of RELIC to study the injection effect in an optical lattice. We consider a standing laser-wave with a geometry described in section II. For the considered electron bunch densities the Coulomb repulsion is negligible, namely, the ponderomotive forces exceed by far the space charge forces in the bunch frame. This condition can be written as $\frac{\Omega_0}{\omega_{pe}} >> 1$, where Ω_0 is the electron oscillation frequency in the optical lattice, and ω_{pe}- the plasma frequency.
Initial conditions follow a standard Monte Carlo approach: we randomly draw a Maxwellian electron bunch distribution, centered at a Lorentz factor γ with an energy spread $\delta\gamma/\gamma$, let it interact with the ponderomotive potential of the optical lattice, and follow in time the relevant macroscopic averaged quantities, such as transverse kinetic energies, emittance, longitunidal dispersion, etc.

RELIC operates with reduced units, where the transverse and longitudinal positions of electron are normalized respectively as: $\chi = 2k_\perp x$, $\zeta = k_\parallel z$. The time is normalized to the laser frequency $\tau = \omega_0 t$, and the momentum $\Psi_{\chi,\zeta} = P_{x,z}/m_e c$. The laser intensity is related to

the normalized vector potential as $a_0 = 0.85 \cdot 10^{-9}\lambda_0\sqrt{I}$ with I in W/cm^2 and λ_0 in micron. We assume that the square of the momentum in the vertical direction y is equal to ${a_0}^2(1-\cos(\chi))$. With these considerations and normalisation the dynamic equations are written as:

$$\begin{aligned}\frac{d\zeta}{d\tau} &= \frac{\Psi_\zeta}{\gamma},\\ \frac{d\chi}{d\tau} &= \frac{2\sin(\theta)\Psi_\chi}{\gamma},\\ \frac{d\Psi_\zeta}{d\tau} &= -\frac{dV_{pot}(\chi,\zeta)}{\zeta},\\ \frac{d\Psi_\chi}{d\tau} &= -\frac{dV_{pot}(\chi,\zeta)}{d\chi}.\end{aligned}$$

Due to the potential variation in the linear ramp area, the Lorentz factor is calculated from the condition of momentum conservation as:

$$\gamma = \sqrt{1+{\Psi_\chi}^2+{\Psi_\zeta}^2+a_0^2(1-\cos(\chi))\frac{\zeta}{\zeta_R}} \quad \text{for } z < L_R,$$
$$\gamma = \sqrt{1+{\Psi_\chi}^2+{\Psi_\zeta}^2+a_0^2(1-\cos(\chi))} \quad \text{for } z \geq L_R$$

where $\zeta_R = k_\parallel L_R$ and for $z = 0$ is considered as the beginig of the ramp. The ratio ζ/ζ_R is added in the linear ramp area ($z < L_R$) to take into account the electron deceleration in this step.

Several numerical diagnostics are available: 2D electron longitudinal or transverse phase spaces, instantaneous 1D or 2D electron distribution function, instantaneous electron trajectory or velocity and its correlation with other particles.

B. Interaction parameters

We consider twin laser pulses propagating as presented in Figure 1, each propagating at a grazing angle θ with respect to the electron beam direction taken as the z-axis. Both laser pulses are linearly polarized along the transverse y direction, allowing for perfect interferences. The laser intensities at focus are in the range from 10^{15} to 10^{18} W/cm^2, and laser wavelengths are typically 800 nm or 1.05 μm. The laser pulse duration has a value varying from a few femtoseconds or a few hundreds of femtoseconds. This allows one to obtain a sufficiently large interaction region enabling electron to make several oscillations and trigger the Raman instability.

The electron bunch, it can be delivered either by a laser plasma accelerator or by a conventional RF linear accelerator (LINAC). The major advantage of laser acceleration is to provide extremely short bunches of electrons, with a corresponding energy of a few ten to hundreds MeV with a low divergence typically around 2 to 6 mrad, an emittance around 1 mm mrad and a very high current density. Moreover, a synchronization of the traveling optical lattice with the electron beam is very easy if the twin beams are derived from the same laser system, or at least from the same laser oscillator, as the intense laser inducing the wakefield acceleration. At the same time LPA allows one to place the lattice at a short millimeter distance from the accelerator which strongly limits the effects of transverse divergence of the electron bunch. A LINAC system, can deliver a low energy electron bunch around a few tens MeV with energy spreads below 1%, and a normalized emittance down to below 1 mm mrad. Moreover, a LINAC system allows one to control the electron focal position of electrons and has a good position stability. However, the coupling between the incident electron bunch, and the interference region of the twin laser beams may present a challenge for the synchronization.

For the numerical tests, we consider an electron bunch of 30 MeV with an energy spread $\delta\gamma/\gamma = 0.01$, an emittance around 1 mm mrad and a divergence of 2 mrad propagating along the z axis. This corresponds to a transverse size of electron bunch $\sigma_x = 8.33$ μm at the begining of the ramp. Such an electron bunch is not achievable at this time with the LPA technology, but the rapid progress in this area will allow in future to make a monoenergetic electron bunch with low divergence and high stability using injection into a density gradient [22] and plasma lenses [18, 19]. The intensity of the optical lattice is considered $\sim 1 \cdot 10^{17}$ W/cm^2 with the wavelength $\lambda_0 = 800$ nm. The incidence angle of the laser waves to the electron propagation direction are chosen to be $\theta = 10°$, which gives a width of potential wells $L_W = 2.3$ μm. With these simulation parameters, the ratio $\sigma_x/L_W = 3.61$ corresponds to a multi-wells injection at the begining of the ramp zone.

IV. ELECTRON TRANSVERSE PHASE SPACE DYNAMICS

A. Electron trapping rate

From the theory and numerical studies of the Raman XFEL, both the gain and the scattered field at saturation depend on two basic quantities: the charge density of electrons in the wells, and their average transverse kinetic energy. Before injection, the charge density depends only on the total bunch charge, duration, and spatial cross-section. The ponderomotive force can trap an electron in the bottom of the potential wells if:

$$\frac{\gamma}{2}\left(\frac{v_x}{c}\right)^2 + \frac{a_0^2}{\gamma}\sin^2(2k_\perp x) < \frac{a_0^2}{\gamma} \qquad (3)$$

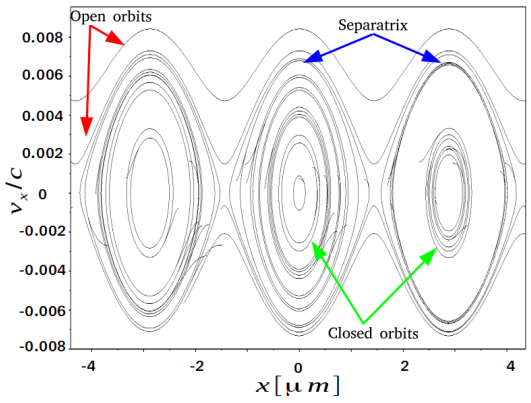

FIG. 3. Electron trajectories in the transverse phase space $(x, v_x/c)$. Simulation parameters: $\epsilon_N = 1$ mm mrad, $\Sigma = 2$ mrad, $a_0 = 0.3$, $L_R = 200$ μm, $\theta = 10°$, $\lambda = 800$ nm.

where v_x is the transverse electron velocity and $\frac{a_0^2}{\gamma}$ the maximum height or effective energy of the potential well.

Figure 3 shows the phase space trajectories of 80 test particles chosen randomly after the injection into the optical lattice. Particles satisfying the trapped condition (3) are confined inside the ponderomotive potential well and follow elliptical closed orbits, while those whose energy is equal to $\frac{a_0^2}{\gamma}$ follow the separatrix in phase space $(x, v_x/c)$. The maximum width of the separatrix in the vertical direction is $\sqrt{2}a_0/\gamma$ is in good agreement with the trapped condition (3). Electrons are trapped in the potential wells, or pass through the maxima of another lateral well where they can be trapped and then contribute to the amplification process. In the case where the electron transverse velocity is much higher than the maximum poderomotive potential well i.e $(v_x/c > \sqrt{2}a_0/\gamma)$, the electron follows an open orbit, and can then escape either left or right depending on its initial velocity.

We want to know the dependence of the trapping rate on physical parameters of the optical lattice and on those of the electron bunch. The trapping rate at the end of the interaction area is defined as:

$$\eta_0 = \frac{n_t}{n_e} \tag{4}$$

where n_e is the total number of electrons injected into the optical lattice, and n_t is the total number of electrons which satisfies the trapped condition (3).

Figure 4(a) shows the trapping rate as a function of the normalized vector potential of the optical lattice for different electron energies. The trapping rate grows linearly with a_0 and can reach values close to 100% for low electron energies. According to Figure 4(b), the trapping rate decreases with electron bunch energy for a

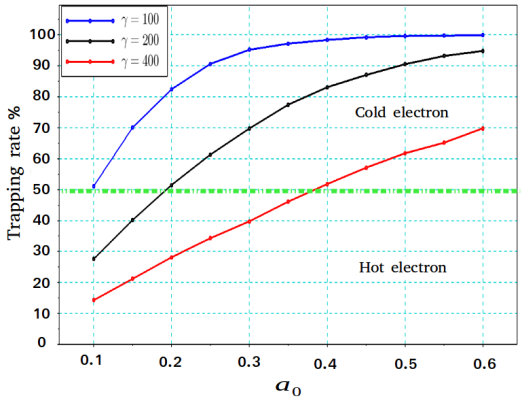

(a)Electron trapping rate as a function of laser intensity for different electron energies. Simulation parameters: $\epsilon_N = 1$ mm mrad, $\Sigma = 2$ mrad, $L_R = 200$ μm, $\theta = 10°$, $\lambda = 800$ nm.

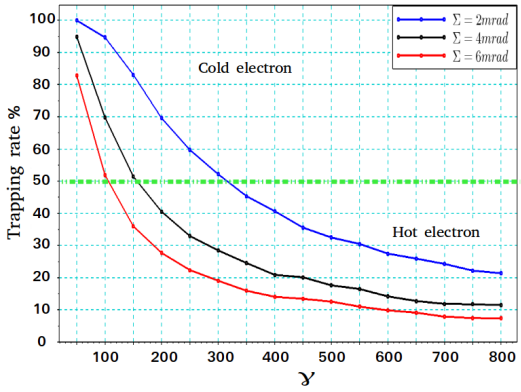

(b)Electron trapping rate as a function of electron kinetic energy for different divergences of electron bunch. Simulation parameters: $\epsilon_N = 1$ mm mrad, $a_0 = 0.3$, $L_R = 200$ μm, $\theta = 10°$, $\lambda = 800$ nm.

FIG. 4. Trapping rates for different physical parameters. The green dashed lines delineate the cold and hot electron regimes.

constant laser intensity. It also decreases as the electron beam divergence Σ increases. These figures illustrate the difference between two regimes, a 'hot electron' regime where the average transverse kinetic energy in a bunch higher than the height a_0^2/γ of the potential well, and a cold electron regime in the opposite case. The light potential being inversely proportional to the Lorentz factor, the curve in Figure 4(b) starts in a cold regime on the left part, with almost full trapping, and moves gradually to a hot regime on the right part, with a vanishing trapping rate. Similarly, the divergence Σ of a bunch increases quadratically the transverse kinetic energy. The upper curve in Figure 4(b) corresponds to coldest electrons. The transition between the cold (low transverse velocity) and hot particle regimes corresponds to a typi-

cal trapping rate of 50%. Empirically, this limit can be shown to be characterized by the parameter :

$$\Upsilon = \frac{2a_0}{\gamma\Sigma}, \tag{5}$$

and that a typical trapping rate of 50% corresponds to $\Upsilon = 10^{-3}$, where Σ should be given in mrad.

We have checked numerically that the trapping rate is almost independent on the electron bunch dispersion $\delta\gamma/\gamma$, which is an essential parameter of Free Electron Lasers. Note that the trapping condition (3) is valid only if the total interaction length, sum of the length of the ramp and plateau area ($L_i = L_R + z_{plateau}$), is greater than the spatial electron oscillation period L_O (see Figure 2(b)). Otherwise, the particles are compressed by the ponderomotive force, but it is no longer possible to define a clear separatrix in phase space.

Trapping is defined here only with respect to the x-direction. It would be straightforward to generalize this to a two-dimensionnal trapping. Indeed, it is conceivable in the future studies to use another couple of laser beams which would confine electrons along the open direction of the lattice y. The coupling between the 4 waves provide a special geometry of the optical lattice with multiple optical channels. This would strongly improve the electron trapping rate, and result in a more collimated electron beam. In addition it would offer the advantage of adding a degree of freedom to control the polarization of X-ray light, by controlling the polarization and dephasing of the y-direction lasers.

B. Phase space dynamics

The electron bunch dynamics in time can be represented by the particle coordinates- the position and the velocity in the transverse plane. Moreover, we can track the particle motion in the optical lattice and its propagation from diagnostic plane. Finally, we estimate the electron bunch parameters: emittance and the energy exchange between the electron bunch and the Raman scattered wave over the interaction time.

Figure 5 shows the evolution of the electron bunch in the transverse phase space for different interaction times in a single potential well. At the initial state, electrons with the same transverse velocities are uniformly distributed in the transverse phase space $(x, v_x/c)$ between $(-L_W/2, L_W/2)$ Fig. 5(a). The electron beam begins to oscillate under the influence of the ponderomotive force in Figure 5(b). After one electron oscillation period, the trapped particles are confined inside the ponderomotive potential well while those with the transverse energy much higher than the maximum poderomotive potential well escape either left or right from the potential well (see Figure 5(c)).

One can see in Figure 5(c) that the transverse phase space is filled inhomogeneously with several narrow arms. To explain how the electron phase space evolves with the interaction length, we evaluate the electron oscillation frequency. Under the trapping condition (Eq. 3), the total transverse Hamiltonian H of an electron can be presented as the sum of the transverse kinetic energy and the effective potential energy:

$$H = \frac{\gamma m_e v_x^2}{2} + \frac{m_e c^2 a_0^2}{\gamma}\sin^2(2k_\perp x). \tag{6}$$

By solving the electron dynamic equations, we find the frequency of small-amplitude electron oscillations as:

$$\frac{\Omega_0}{\omega_0} = \frac{2a_0\sin(\theta)}{\gamma}. \tag{7}$$

Large amplitude electron oscillations are anharmonic, the frequency depends on the excursion parameter ξ, which characterizes the initial electron energy and depends on its initial position and transverse velocity as:

$$\xi^2 = \frac{\gamma^2}{a_0^2}\left(\frac{v_x}{c}\right)^2 + sin^2(2k_\perp x), \tag{8}$$

with $\xi < 1$ for the trapped particle. The electron oscillation frequency can then be written as: $\Omega = \Omega_0 \cdot f(\xi)$ where $f(\xi)$ is a scalar function [12]. The trapped particles with different energies, oscillate at different frequencies. The particles with lowest values of ξ are confined at the bottom of the potential well while those with a higher ξ are found on the edges. The oscillation frequency decreases as the particle energy (Hamiltonian) increases. The particles at the bottom follow short closed elliptical trajectories while thoses trapped at the edges of the potential well follow larger closed elliptical trajectories limited by the separatrix (see Figure 3). A differential rotation of the trapped particles at the bottom of the potential well and those trapped on the edges causes the galactic-like arms which can be seen in the transverse phase space $(x, v_x/c)$ Fig (5(c), 5(d)). The number of arms n_r is equal to the number of rotation periods $n_r = \frac{L_i}{L_O}$. A new arm is created on each mean oscillation period of the total number of the trapped particles and for long interaction length, the transverse phase space $(x, v_x/c)$ can be completely filled (see Figure 5(d)).
According to our numerical study, a criterion to reach almost homogeneous electron distribution in the phase space is:

$$\frac{L_i}{L_W} > 6\frac{\gamma}{a_0}.$$

One then define the minimal homogenization time as :

$$t_s = 6\frac{\gamma L_W}{a_0 c}. \tag{9}$$

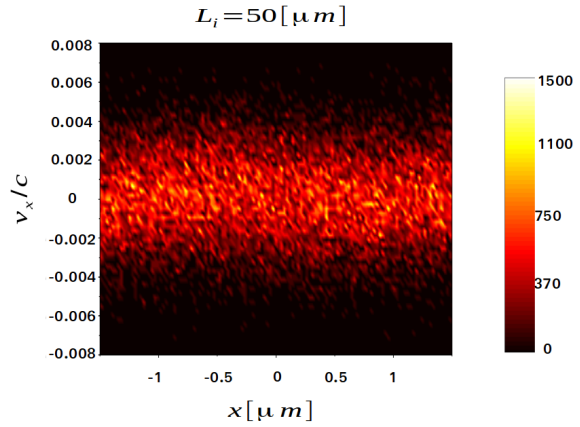

(a)Transverse phase space $(x, v_x/c)$ after 50 μm in a single potential well.

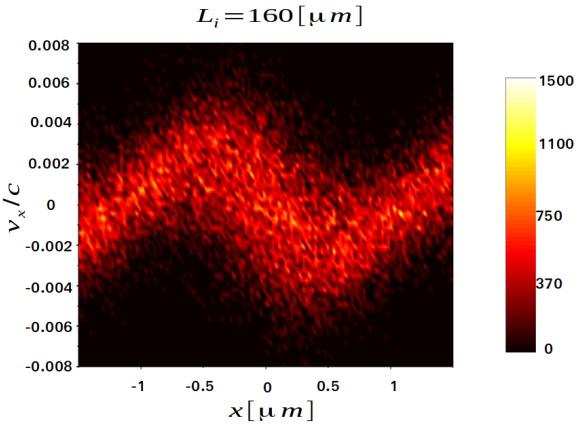

(b)Transverse phase space $(x, v_x/c)$ after 160 μm in a single potential well.

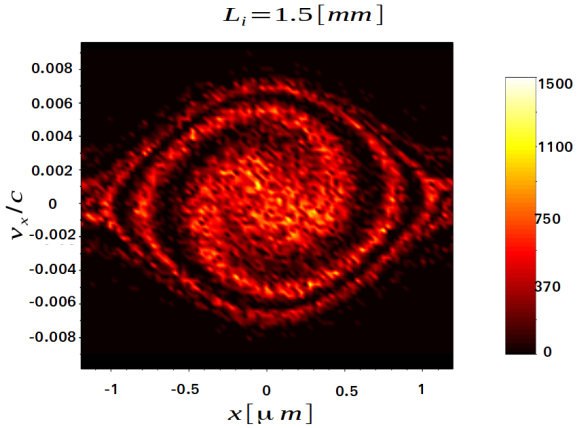

(c)Transverse phase space $(x, v_x/c)$ after 1.5 mm in a single potential well.

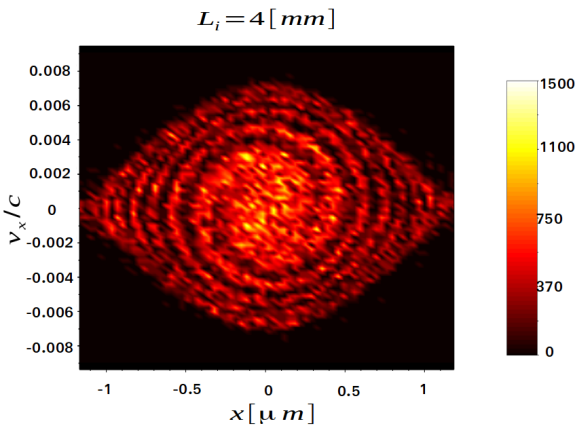

(d)Transverse phase space $(x, v_x/c)$ after 4 mm in a single potential well.

FIG. 5. Transverse phase space $(x, v_x)/c$ for differents interaction length . Simulation parameters: $\gamma = 60, \epsilon_N = 1$, $\Sigma = 2$ mrad, $a_0 = 0.3$, $L_R = 200$ μm, $\theta = 10°$, $\lambda = 800$ nm. Note: free propagation $a_0 = 0$.

We can compare the electron bunch distribution for cases of free propagation and through the optical lattice. Figure 6 shows the transverse electron distribution after 1.5 mm free propagation (blue curve) and interaction with the optical lattice (red curve). The peaks in the latter case are due to the electron bunch oscillations in the optical lattice. Electrons are compressed in the potential wells and each peak appearing on the transverse distribution function is interpreted as a trace of the trapped electrons in the potential well. Each peak in the red curve in Figure 6 corresponds to the position of an arm in the transverse electron phase space in Figure 5(c). The position of peaks can be explained as follows. For a long interaction distance through the optical lattice, electron distribution becomes smoother rassembling a large Gaussian distribution with several peaks which correspond to a filled transverse electron phase space by arms (see Fig 5(d)). For a constant interaction length, the electron rotation frequency increases with the laser intensity thus making several arms in the transverse phase space and smoothing the electron distribution over a short interaction distance.

C. Phase space dynamics : Twiss parameter analysis

Evolution of macroscopic features of electron bunches in conventional accelerators or storage rings is discussed in papers and textbooks. A particle beam can be represented by an elliptical distribution in phase space. The surfaces of these ellipses in the transverse phase space $(x, v_x/c)$ define the beam emittance. It increases with

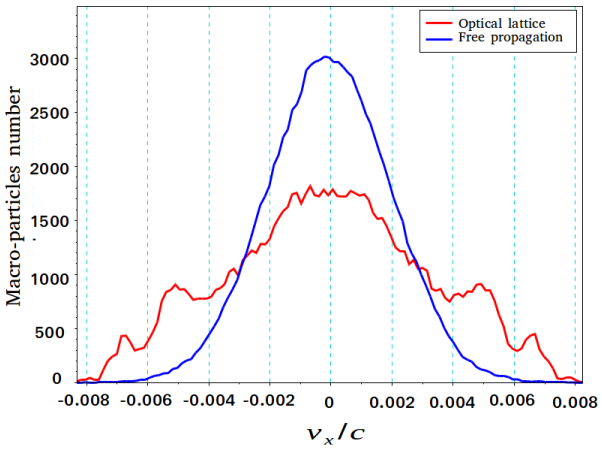

FIG. 6. Transverse electron distribution. Blue curve: transverse distribution in the case of free propagation. Red curve: transverse electron distribution through optical lattice after interaction area $L_i = 1.5$ mm.

the propagation distance because electrons with different energies rotate with different velocities in the transverse phase space [23, 24]. In accelerator physics, the emittance evolution over time is characterized by the Twiss functions. This formalism was applied for studies of LPA in Refs. [24, 25]. The ellipse fitting the beam distribution of the trapped electrons can be written as:

$$\varepsilon_{n,RMS} = \gamma_T x^2 + 2\alpha_T x \cdot (v_x/c) + \beta_T (v_x/c)^2,$$

where (γ_T, α_T, β_T) are the Twiss parameters, which can be found through the normalised emittance as:

$$\begin{aligned} \beta_T &= < x^2 >_t / \varepsilon_{n,RMS}, \\ \gamma_T &= < (v_x/c)^2 >_t / \varepsilon_{n,RMS}, \\ \alpha_T &= < x \cdot (v_x/c) >_t / \varepsilon_{n,RMS}, \end{aligned}$$

where the Twiss parameter α_T describes the correlation between the transverse position and velocity.
The same description can be used to get quantitative insights into the evolution of the fraction of electrons that remains trapped in each of the light potential wells. For a simple analytical model, one can write the electron distribution function of the trapped particles n_t in a single well as a function of the mean electron excursion Eq.(8):

$$< \xi_0 >= \sum_{n_t} \xi.$$

For a homogeneous electron distribution function in the longitudinal direction, it can be written as: $f(x, v_x, z, v_z) = f(< \xi_0 >, z, v_z)$, where

$$< \xi_0 >= \left[\frac{\gamma^2}{a_0^2} \sum_{i=1}^{n_t} \frac{(v_{xi}/c)^2}{n_t} + 1 - \sum_{i=1}^{n_t} \cos(2k_\perp x_i) \right]^{1/2} \quad (10)$$

The trapped electrons are limited by the separatrix in the transverse phase space $(x, v_x/c)$, then one can estimate the mean root square emittance into a single optical well ($\frac{-L_W}{2} \leq x \leq \frac{L_W}{2}$) as:

$$\varepsilon_{n,RMS} = \sqrt{< x^2 >_t \cdot < (v_x/c)^2 >_t - < x \cdot v_x/c >_t^2}$$

$$< x \cdot v_x/c >_t = \frac{\sum_{i=1}^{n_t} x_i \cdot (v_{xi}/c)}{n_t} - \frac{\sum_{i=1}^{n_t} x_i \cdot \sum_{i=1}^{n_t} (v_{xi}/c)}{n_t^2}$$

where the index "t" indicates that the sum is performed over the trapped particles.

Figure 7(a) shows the evolution of the mean root square electron excursion ξ_0 as a function of the ramp length for two different electron bunches. The maximal value of ξ_0 does not exceed 1. The excursion ξ_0 exhibits damping oscillations for $\Gamma_{ad} =]0, 1]$ and then remains constant. The variation of the excursion ξ_0 in the first electron oscillation period is mainly due to the correlation parameter α_T. The evolution of the Twiss parameter in time for $\gamma = 60$, is illustrated in Fig 7(b). The amplitude of α_T is the highest in the first oscillation period $L_O = 650$ μm, is exhibits damping oscillations and then tends to its minimum value exponentially. The red curve in the inset shows the analytical fit described by the following equation: $\alpha_T(z) = Ae^{-D \cdot z} + E$, where A is the amplitude at $z = L_O$, c is the speed of light, $D = t_s c$ is the damping factor and E is the minimum value.
Numerically the lowest value of α_T is obtained approximately after 8 electron oscillation periods which is in good agreement with Equation (9).

D. Transverse and longitudinal electron bunch kinetic energy: from fast to adiabatic injection

In this part, we study the transverse phase space at the end of the ramp for two injection regimes: fast injection $\Gamma_{ad} < 1$ and adiabatic injection $\Gamma_{ad} \geq 1$.

Figure 8 shows transverse phase spaces for different adiabatic parameters obtained by varying the ramp length. The electron beam here occupies the width of three optical wells. Figure 8(a), shows the the transverse phase space at the end of the ramp length for a typical case of fast injection $\Gamma_{Ad} = 0.16$ and Figure 8(b)-for an adiabatic one $\Gamma_{Ad} = 1$. The electron beam is totally cut and most electrons are trapped in potential wells in the ramp region before reaching the plateau for an adiabatic injection. In contrast, in the case of fast injection the beam oscillates homogeneously in the transverse phase space $(x, v_x/c)$.

To estimate the variation of the transverse velocity in the linear ramp region, we consider the dynamic equation:

$$\frac{dv_x}{dt} = -\frac{dH}{dx} \quad (11)$$

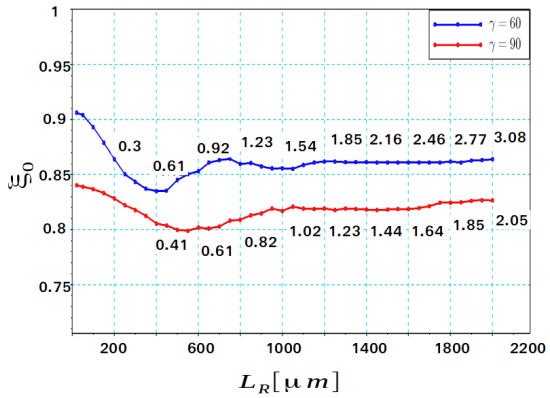

(a)Variation of the electron bunch excursion as a function of the ramp length for two different electron bunch energies. Blue curve: $\gamma = 60$. Red curve $\gamma = 90$. The numbers on the curves represent the corresponding adiabatic parameters Γ_{ad}. Simulation parameters: $a_0 = 0.3$, $\epsilon_N = 1$, $\Sigma = 2$ mrad, $L_R = 100$ μm $a_0 = 0.3$, $\theta = 10°$, $\lambda = 800$ nm,

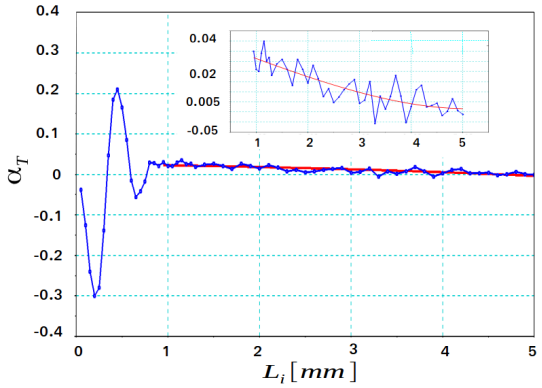

(b)Variation of the Twiss parameters α_t over time. Simulation parameters:$a_0 = 0.3$, $\gamma = 60$, $\epsilon_N = 1$, $\Sigma = 2$ mrad, $L_R = 100$ μm $a_0 = 0.3$, $\theta = 10°$, $\lambda = 800$ nm,

FIG. 7. Evolution of the mean electron excursion ξ_0 and of the Twiss parameter α_t as a function of the ramp length.

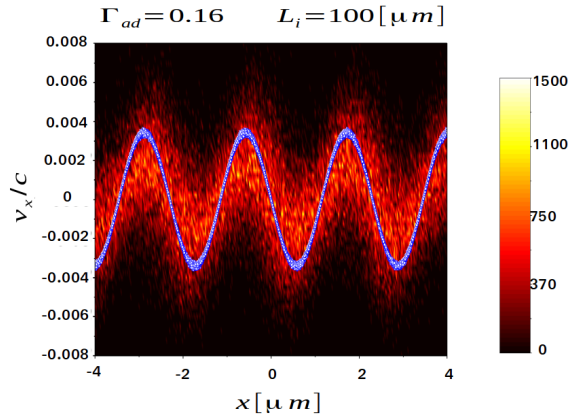

(a)Fast injection: Transverse phase space at the end of the linear ramp. Simulation parameters: $\gamma = 60$, $\epsilon_N = 1$, $\Sigma = 2$ mrad, $L_R = 100$ μm, $a_0 = 0.3$, $\theta = 10°$, $\lambda = 800$ nm, $\Gamma_{ad} = 0.16$

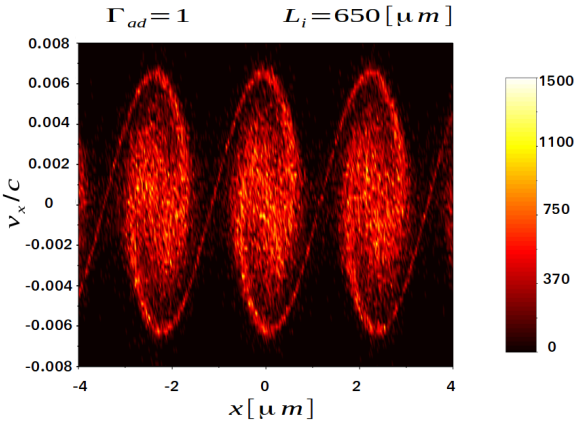

(b)Adiabatic injection: Transverse phase space at the end of the linear ramp. Simulation parameters: $\gamma = 60$, $\epsilon_N = 1$, $\Sigma = 2$ mrad, $L_R = 650$ μm, $a_0 = 0.3$, $\theta = 10°$, $\lambda = 800$ nm, $\Gamma_{ad} = 1$

FIG. 8. Transverse phase space for fast and adiabatic injections at the end of the linear ramp region.

where H is the transverse Hamiltonian defined in Equation 6. Integrating this equation over time we find the electron transverse velocity at $t_{inj} = L_R/c$,

$$\frac{v_x(t_{inj})}{c} = \frac{2a_0^2}{\gamma^2}\sin(2k_\perp x)\cos(2k_\perp x)\frac{L_R}{L_W} \qquad (12)$$

As shown in Figure 8(a), the blue line, corresponding to the analytical solution of Equation (12), is in good agreement with the numerical simulation until $\Gamma_{ad} \sim 0.5$. A higher order of the analytical description should be considered to represent the evolution of the transverse phase space in time for $\Gamma_{ad} > 0.5$.

We now analyze the variation of the electron density and the transverse energy for different injection times $t_{inj} = L_R/c$. The numbers on the curves in Figure 9(a) represent the corresponding adiabatic parameters Γ_{ad}. The electron density increases as a function of the injection time and becomes constant for $\Gamma_{ad} \sim 1$, whereas the transverse kinetic energy, shown in Figure 9(b) decreases. This behavior can be explained as follows: in the case of fast injection, electrons are submitted violently to the ponderomotive force. They are slowed rapidly, deflected transversely and compressed in the potential well. They gain the transverse velocity which modifies their transverse kinetic energy which could then exceed the maximum effective energy of the potential allowing them to escape from ponderomotive potential wells. Oppositely,

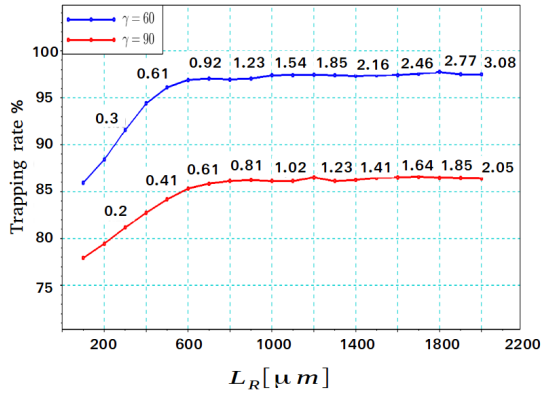

(a)Trapping rate as a function of the ramp length for different electron energies. Simulation parameters: $a_0 = 0.3$; $\lambda = 800$ nm; $\theta = 10°$; $\Sigma = 2$ mrad;$\delta\gamma/\gamma = 0.01$; Macro-particles number is 10^5.

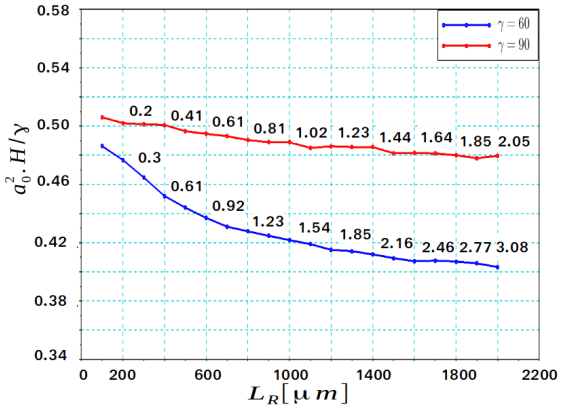

(b)Transverse energy as function of the ramp length for different electron energy. Simulation parameters: $a_0 = 0.3$; $\lambda = 800$ nm; $\theta = 10°$; $\Sigma = 2$ mrad;$\delta\gamma/\gamma = 0.01$; Macro-particles number is 10^5.

FIG. 9. Electron trapping rate and transverse electron energy as a function of the ramp length for different electron energy.

in the case of the adiabatic injection, where electrons are slowly compressed while conserving their energy. Figure 9(b) shows a variation of the total kinetic energy for two different electron beam energies. As shown the maximum value of the blue curve ($\gamma = 60$) is less than 0.5 which means that most electrons are trapped in the bottom of the potential well, while the maximum value of the green curve ($\gamma = 90$) is approximatly equal to 0.5 meaning that the electron beam is uniformly distributed in the ponderomotive potential well.
From Equations (3) and (12), we calculate the RMS value of the transverse velocity of the trapped particle,

$$< v_x(t_{inj})/c >= \frac{a_0^2}{\gamma^2}\frac{L_R}{L_W} = \sqrt{2}\frac{a_0}{\gamma} \tag{13}$$

The ramp length corresponding to transition from the fast to adiabatic injection $\Gamma_{ad} = 1$ reads

$$L_R = \sqrt{2}\frac{\gamma L_W}{a_0} \tag{14}$$

which is in good agreement with numerical calculations.

Let us now estimate a variation of the longitudinal kinetic energy of an electron assuming that $v_z >> v_x$. It can be written as:

$$m_e c^2 \frac{d\gamma}{dt} = -v_z \frac{dP_z}{dt} \tag{15}$$

where P_z is the longitudinal momentum. According to the expression for the force in the longitudinal direction we have:

$$\frac{dP_z}{dt} = -\frac{m_e c^2 a_0^2}{2\gamma L_R}(1 - \cos(2k_\perp x)) \tag{16}$$

Combining Equations 15 and 16, substituting v_z by dz/dt and integrating up to $z = [0\ L_R]$ we find

$$\gamma_f^2 - \gamma_i^2 = -a_0^2(1 - cos(2k_\perp \tilde{x})) \tag{17}$$

where γ_i and γ_f are the Lorentz factors at the beginning and the end of the linear ramp and $\tilde{x}$ is the transverse position of the particle at the end of the injection zone. Assuming a small energy variation and summing over all trapped particles, we find that the mean square root of the maximum deceleration of the particle at $z = L_R$ reads:

$$< \frac{\Delta\gamma}{\gamma_i} >= -G(\frac{a_0}{\gamma_i})^2, \tag{18}$$

where

$$G = \frac{1}{2n_t}\sum_{i=1}^{i=n_t} G_i,$$

where n_t is the total number of the trapped particles, $G_i = [0, 1]$ is a constant depending on the transverse position $\tilde{x}$ of the particle at time $t = L_R/c$. For $G_i = 0$, the particle is trapped at the bottom of the potential well without loss of longitudinal kinetic energy, while for $G_i = 1$, the particle is trapped at the maximum edge of the ponderomotive potential well and loses their kinetic energy.

Figure 10 shows the logarithmic mean square root deceleration of an electron bunch injected into the optical lattice as a function of electron bunch energy. The deceleration decreases when electron energy increases. The numerical calculation results represented by dark dots are in good agreement with the analytical estimations represented by the red curve. The lost longitudinal energy in the ramp step is transferred to the transverse electron energy. The electron transverse oscillations are

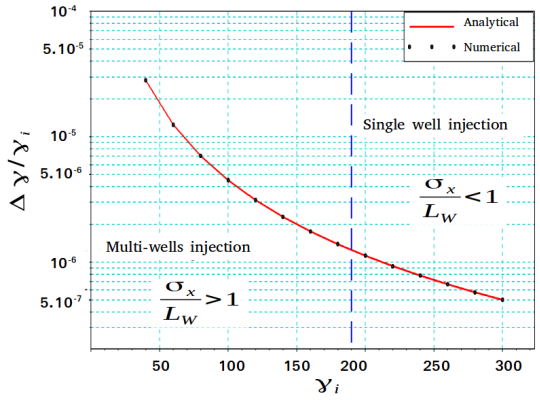

FIG. 10. Longitudinal velocity deceleration as a function of electron energy. Simulation parameters: $a_0 = 0.3$; $\lambda = 800$ nm; $\theta = 10°$; $\Sigma = 2$ mrad;$\delta\gamma/\gamma = 0.01$; $L_R = 450$ μm; the number of macro-particles is 10^5.

origin of the radiation. In the case of single well injection, if the electron bunch is smaller than a half width of the potential well $\sigma_x/L_W << 0.5$, most of the electrons propagate in the potential well without kinetic energy loss. To fill completely the potential wells with electrons, one can therefore adapt the corresponding optical lattice geometry for each electron bunch. For example, for higher electron energies, one can increase the laser intensity to slow and trap electrons, and also increase the incidence angle θ between the laser pulse and the electron bunch. The increase of the incidence angle θ increases therefore the traveling wave velocity of the optical lattice as $V_{tw} = c/\cos\theta$. This can be controlled by the delay betwen the laser generated electron bunch in LWFA and the optical lattice or by reducing the traveling wave velocity close to the speed of light by some specific rotation of the grating compressors of Chirped Pulse Amplification (CPA) lasers system [26].

V. INJECTION EFFECTS ON THE SCATTERED FIELD AMPLIFICATION

We now explore the extent to which the dynamical effects studied above may affect the coherent scattering and amplification of X-ray radiation. We first recapitulate the main features of the Raman XFEL of relevance for the study, obtained with the EWOK amplification code [11], and present several numerical examples.

The Raman-XFEL can be viewed as a parametric four wave interaction, involving two electromagnetic pump waves with frequency ω_0, a collective mode created by electrons oscillating transversely in the potential well at the frequency $\Omega \approx \Omega_0$, and an outgoing Stokes wave with the frequency ω_s. The beat between the incident laser waves and the scattered wave in the electron rest frame produces a ponderomotive potential oscillating at the frequency Ω, that leads to a gradual electron bunching. This loop triggers an instability, analogous to Raman scattering in plasmas, with the difference that the electron mode is not an electrostatic Langmuir wave but a collective transverse oscillation in the light channels. It is also and analogous to the Free Electron Laser effect in the Compton regime, with the difference that bunching is not purely longitudinal and static, but oscillating and both transverse and longitudinal. Bunching is then characterized by a specific antisymmetric profile inside the each light channel [11].

The electromagnetic Particle-In-Cell code EWOK was designed to handle the specificities of the Raman XFEL scheme, especially the periodic boundary conditions for both the incident and the scattered waves. Specifically, any particle reaching one side of the calculation box is re-introduced at the opposite side with the same velocity vector. EWOK operates in the average electron frame, while RELIC is written in the laboratory frame and considers no specific boundaries. As a result, the ramp is modelled in EWOK through a gradual increase in time of the laser waves, that remain constant throughout the box to respect the boundary conditions; this makes EWOK unable to study the energy dispersion effects as in section IV. However, the calculations presented below were performed in the conditions where such longitunidal dispersion effects are negligible.

The chosen conditions are similar to those of Ref. [11], with an electron bunch occupying the entire width of the optical lattice $\sigma_x/L_W = 1$, an average Lorentz factor $\gamma = 10$, an energy spread $\delta\gamma/\gamma = 10^{-4}$ and a normalized electron density $n_e/n_c = 8 \cdot 10^{-5}$. The optical lattice is created by two laser beams with identical amplitudes $a_0 = 0.1$ and an incident angle $\theta = 10°$. The transverse electron beam velocity is chosen not to exceed the separatrix $v_x/c < \sqrt{2}a_0/\gamma$, so that the majority of electrons satisfy the trapping condition (3). The size of the simulation box is defined as $(5\lambda_0 \times 70.2\lambda_0)$ in the transverse and longitudinal directions respectively. This specific box size allows to satisfy the periodic boundary conditions along the z-axis for the laser and scattered waves, whereas the box boundaries are absorbing in the x-direction. We use $2 \cdot 10^6$ macro-particles in the optical lattice. For reproducibility, we do not let the scattered signal start from numerical noise, but impose a low initial seed, at a level of $a_{seed} = 10^{-6}$.

As a first test case, we simulate the effect on the amplification of a ramp of length $L_R = 20\ c\tau_0$, followed by a plateau area of 2000 $c\tau_0$. Figure 11(a) shows the evolution of the scattered field amplitude in time, in the electron rest frame. One can see the exponential growth of the signal in the normalized time $t = [80, 650]\tau_0$, modulations in the rising edge of the gain curve, correspond-

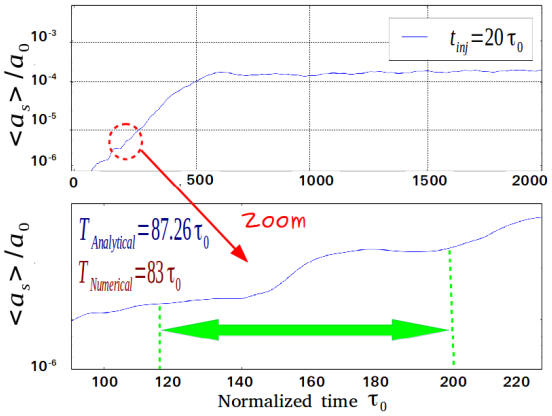

FIG. 11. Amplification of the scattered field in time. Simulation parameters: $a_0 = 0.1$; $\lambda = 1\ \mu m$; $\theta = 10°$; $a_{seed} = 10^{-6}$; $\Sigma = 3\ mrad$;$\gamma = 10$; $\beta_\perp = 0.1$; $\delta\gamma/\gamma = 10^{-4}$; $t_{inj} = 20\ \tau_0$. Normalized electron density is $n_e = 8 \cdot 10^{-5}$. Macro-particles number is $2 \cdot 10^6$.

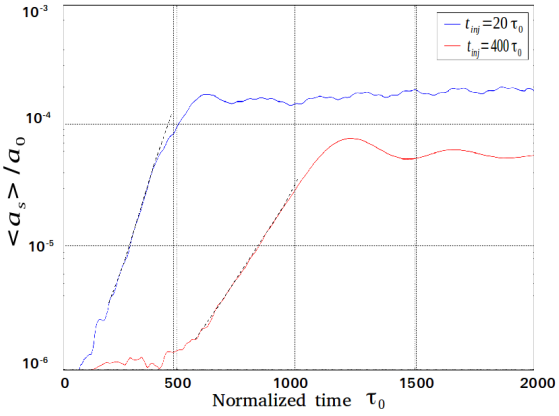

FIG. 12. Scattered field growth for different characteristic durations of injection of the electron bunch into the optical lattice. Simulation parameters: $a_0 = 0.1$; $\lambda = 1\ \mu m$; $\theta = 10°$; $a_{seed} = 10^{-6}$; $\Sigma = 3\ mrad$;$\gamma = 10$; $\beta_\perp = 0.1$; $\delta\gamma/\gamma = 10^{-4}$. Normalized electron density is $n_e = 8 \cdot 10^{-5}$. Macro-particles number is $2 \cdot 10^5$. Blue curve: time injection $t_{inj} = 20\ \tau_0$. Red curve: time injection $t_{inj} = 400\ \tau_0$.

ing to the beginning of the constant intensity interaction area. Figure 11(b) presents a zoom on the time interval $t = [100, 650]\tau_0$, showing two such oscillations superimposed on the exponential growth; the period can be measured to be $87\tau_0$, corresponding almost exactly to the period $T = 2\pi/\gamma\Omega_0$ in the electron rest frame. Note that the signal may actually decrease, implying that electrons recapture energy from the electromagnetic wave during a fraction of each period. A modulation at Ω_0 of the signal wave at frequency $\omega_0 - \Omega_0$ might correspond to signal components at either $\omega_0 - 2\Omega_0$ or ω_0; indeed, a time-frequency analysis of the scattered wave shown in 11(a) does exhibit a significant contribution of the Compton mode ω_0 . We observe therefore a competition between the Raman and a Compton modes, even though the latter is not phase-matched. While a full discussion of the mode competition, and a detailed comparison between the features of Compton and Raman FELs with laser undulators is beyond the scope of the present study, we propose the following interpretation. Following injection and the onset of amplification, one has simultaneously two kinds of bunching phenomena. The first one is the micro-bunching in real space, with the anti-symmetric characteristics explained in [11]; the second one is the bunching in transverse phase space $(x, v_x/c)$ resulting from the injection, displaying an $(x, -x)$ symmetry, and rotating at angular frequency Ω_0. The combined action of the two bunching phenomena leads therefore to a variation in the amplification conditions, with an overall period $2\pi/\Omega_0$. The Raman mode eventually dominates, in part due to the gradual homogenization of the phase space distribution, and also due to the limited coherence (dephasing) length of the Compton mode resulting from its non-phase matched character. One may note that the time at which amplification saturates, i.e. 650 laser periods for the first curves, turns out to correspond also the homogenization time as defined in Eq. (9). This is also consistent with the gradual disappearance of oscillations in the growth curve in the upper part of the latter.

Let us now study the injection effect on the growth rate. For this we keep the same simulation parameters as above, vary the duration of injection, and then allow for identical length of interaction L_i . Figure 12 shows the scattered field amplitude for the case of fast injection (blue curve) and of adiabatic injection (red curve). Two major observations can be made: the growth rate appears higher for fast injection than for adiabatic injection, leading to an earlier onset of saturation; and the saturation level itself is higher. Least-square fits of the amplification yield a growth rate of $1.46 \cdot 10^{-2}\omega_0$ for the fast injection curve and $6.83 \cdot 10^{-3}\omega_0$ for the adiabatic one; and a saturation level at $2 \cdot 10^{-4}$ for the former, and $6.95 \cdot 10^{-5}$ for the latter. These features are explained with the kinetic theory of the Raman amplification [12]. This model takes into account the finite longitudinal energy spread, the bunch density of electrons trapped in the wells, and the relativistic parameter a_0 of the incident twin laser beams. The electron distribution function in transverse phase space is considered to be a 'water-bag', that is, a unit step function between 0 and a maximum excursion ξ_0; the final expressions are however derived for $\xi_0 = 1$, meaning a homogeneous and total fill up of the phase space volume within the separatrix. The spatial gain from this kinetic theory reads as :

$$g = \frac{4\pi\sqrt{3}}{\lambda}\left(\frac{a_0^2 n_0}{12\pi\gamma^3(1-\cos\theta)^2}\right)^{1/3}. \qquad (19)$$

The gain increases with the field amplitude a_0, and the bunch density n_0, which is directly proportional to

the trapping rate displayed in figure 9(a). However, the trapping rate is higher in the case of adiabatic injection, which is opposite to that of the gain. The dominant effect therefore is not the density effect, but the transverse temperature of the electron bunch.

We have shown in Figure 7(a) that the mean excursion decreases as the ramp length is increased. That is, the electron bunch is better confined close to the bottom of the potential well in the adiabatic case, while the electrons occupy the quasi-total height of the potential well in the fast injection case. We therefore conclude that fast injection induces a larger spread of trapped electron excursions, which enables them to oscillate over the entire height of the potential well, although at expense of a reduced trapping ratio. This stimulates the energy transfer between particles and scattered wave, and has therefore a beneficial effect on the growth rate and on the level of coherently scattered light at saturation. These numerical findings demonstrate that injection has a strong effect on the amplification process itself. The full distribution in phase space however requires a kinetic theory. The gain formula (19) should then be revised to take into account the more complex effects resulting from the injection process, such as the reduction of the mean excursion, or remaining inhomegeneities.

VI. SUMMARY

We have presented a numerical study of a relativistic electron bunch, injected into and guided by a high intensity optical lattice. The electron injection plays an important role to set the phase space distribution of the trapped electrons inside ponderomotive channel. The essential parameter is the electron population actually trapped in the optical wells. We studies the trapping rate variation in terms of the main physical parameters, showing a transition between a cold and a hot regime in the transverse dynamics of the electrons. Two main interaction regimes for the injection were unraveled, namely, fast injection and adiabatic injection. Depending on the adiabaticity parameter, we have studied the evolution of the trapping rate, and of the average transverse energy. We have shown that the entrance into the interaction region leads to a reduction of the average longitunidal velocity, accompanied with a broadening (Eq.(18)).

The particle tracing code RELIC was used to find the best injection regime for a set of electron bunch and optical lattice parameters. A use of the particle-in-cell code EWOK then allows us to evaluate the amplification of the Raman X-ray radiation. Our numerical findings point out a need for a more complex kinetic theory for accounting the various injection regimes and the inhomogeneities of the electron distribution function in the optical well. This study can also be used for design of a diagnostics system, very similar to Shintake monitors [27] as used in circular or linear accelerators, based on the spontaneous photons emitted during the electron transverse oscillations. The electron bunch characteristics should then be retrieved with radiation emission from the trapped electron, provided all kinetic effects studied here are taken in account.

Several additional theoretical developments can be envisioned: the light polarisation vector may be an additional degree of freedom for controlling of the electron dynamics. A three-dimensional study is also necessary to take into account the force in the open direction y, leading to possible vertical trapping effects. Beam inhomegeneities, synchronization issues, spatio-temporal effects within so-called inhomogeneous waves, should all be coped with, to match the experimental constraints. Our numerical findings thus present a basis for the future development of a compact Raman X-ray Free Electron Laser, whether from laser-plasma accelerated electrons, or from traditional Radio-Frequency LINACs.

VII. ACKNOWLEDGEMENTS

We acknowledge support of the Agence Nationale de la Recherche under contract LUCEL-X ANR-13-BS04-0011-01, and of the "Investment for the future" program IdEx Université de Bordeaux (ANR-10-IDEX-03-02) through project LAPHIA/Raman X.

[1] J. Gea-Banacloche G. Moore, R. Schlicher, M. Scully, H. Walther, IEEE J. Quantum Electron. **23**, 1558 (1987).
[2] P. Dobiasch, P. Meystre, M.O. Scully, IEEE J. Quantum Electron. **19**, 1812 (1983).
[3] P. Sprangle, B. Hafizi , and J. R. Penano, Phys. Rev. ST Accel. Beams **12**, 050702 (2009).
[4] A. D. Debus, M. Bussmann, M. Siebold, A. Jochmann, U. Schramm, T. E. Cowan, and R. Sauerbrey, Appl. Phys.B **100**, 61 (2010).
[5] Ph. Balcou, Eur. Phys. J. D **59**, 525 (2010).
[6] P. L. Kapitza, and Dirac, in *P. A. M. Mathematical Proceedings of the Cambridge Philosophical Society 1933.*
[7] P.H. Bucksbaum, D.W. Schumacher, and M. Bashkansky, Phys. Rev. Lett. **61**, 1182 (1988).
[8] P. W. Smorenburg, J. H. M. Kanters, A. Lassise, G. J. H. Brussaard, L. P. J. Kamp, and O. J. Luiten, Phys. Rev. A **83**, 063810 (2011).
[9] S. B. Dabagov, A. V. Dik, and E. N. Frolov, Phys. Rev. ST Accel. Beams **18**, 064002 (2015)
[10] I. A. Andriyash, Ph. Balcou, and V. T. Tikhonchuk, Eur. Phys. J. D **65**, 533 (2011).

[11] I. A. Andriyash, E. d'Humières, V. T. Tikhonchuk, and Ph. Balcou, Phys. Rev. Lett. **109**, 244802 (2012).
[12] I. A. Andriyash, V. T. Tikhonchuk, V. Malka, E. d'Humières, and Ph. Balcou, Phys. Rev. ST Accel. Beams **18**, 050704 (2015)
[13] I. A. Andriyash, E. d'Humières, V. T. Tikhonchuk, and Ph. Balcou, Phys. Rev. ST Accel. Beams **16**, 100703 (2013).
[14] T. Tajima, and J. M. Dawson, Phys. Rev. Lett. **43**, 267 (1979).
[15] V. Malka, Phys. Plasmas **19**, 055501 (2012).
[16] J.B. Rosenzweig *et al.*, Nucl. Inst. Meth. A **557**, 8793 (2006).
[17] D. Alesini *et al.*, Nucl. Inst. Meth. A **528**, 586590 (2004).
[18] C. Thaury *et al.*, Nat. Commun. **6**, 6860 (2015)
[19] J. van Tilborg *et al* Phys. Rev. Lett. **18**, 115 (2015).
[20] L. Young and J. Billen, in *PAC03 Proceedings The particle tracking code PARMELA*. 2003 .
[21] K. Floettmann, S. Lidia, P. Piot, *Recent improvements to the ASTRA particle tracking code. Lawrence Berkeley National Laboratory*. 2003.
[22] K. Schmid *et al* Phys. Rev. ST Accel. Beams **13**, 091301 (2010)
[23] K. Floettmann, Phys. Rev. ST Accel. Beams **6**, 034202 (2003).
[24] Migliorati, M. et al. Phys. Rev. ST Accel. Beams **16**, 011302 (2013).
[25] P. Antici, A. Bacci, E. Chiadroni, M. Ferrario, and A.R. Rossi, arXiv:1112.3971
[26] D. Strickland, G. Mourou, Optics Commun. **55**, 447-449 (1985).
[27] T. Shintake, Nucl. Instrum. Methods Phys. Res., Sect. A 311, 453 (1992).